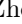



Skeleton-based Group Activity Recognition via Spatial-Temporal Panoramic Graph

Zhengcen Li^{1,2}, Xinle Chang¹, Yueran Li¹, and Jingyong Su^{1,2}

¹ Harbin Institute of Technology, Shenzhen, 518055, China

² Peng Cheng Laboratory, 518055, China

{lizhengcen, changxinle, liyueran}@stu.hit.edu.cn

sujingyong@hit.edu.cn

Abstract. Group Activity Recognition aims to understand collective activities from videos. Existing solutions primarily rely on the RGB modality, which encounters challenges such as background variations, occlusions, motion blurs, and significant computational overhead. Meanwhile, current keypoint-based methods offer a lightweight and informative representation of human motions but necessitate accurate individual annotations and specialized interaction reasoning modules. To address these limitations, we design a panoramic graph that incorporates multi-person skeletons and objects to encapsulate group activity, offering an effective alternative to RGB video. This panoramic graph enables Graph Convolutional Network (GCN) to unify intra-person, inter-person, and person-object interactive modeling through spatial-temporal graph convolutions. In practice, we develop a novel pipeline that extracts skeleton coordinates using pose estimation and tracking algorithms and employ Multi-person Panoramic GCN (MP-GCN) to predict group activities. Extensive experiments on Volleyball and NBA datasets demonstrate that the MP-GCN achieves state-of-the-art performance in both accuracy and efficiency. Notably, our method outperforms RGB-based approaches by using only estimated 2D keypoints as input. Code is available at <https://github.com/mgiant/MP-GCN>.

Keywords: Group activity recognition · Skeleton-based action recognition · Graph convolutional network

1 Introduction

Group Activity Recognition (GAR) is an essential task in video understanding and is widely applied in surveillance, social scene understanding, and sports analysis [11]. The objective of GAR is to classify the collective activity of a group of actors from a given video clip. This task is challenging because an optimal solution requires not only the localization of key roles within a complex scene, but also the effective modeling of spatial-temporal contextual information [25].

The majority of preceding methods for GAR [18, 20, 28, 63, 69] are based on the RGB modality or the fusion of RGB and other modalities. These methods typically employ a CNN backbone to extract individual features with human

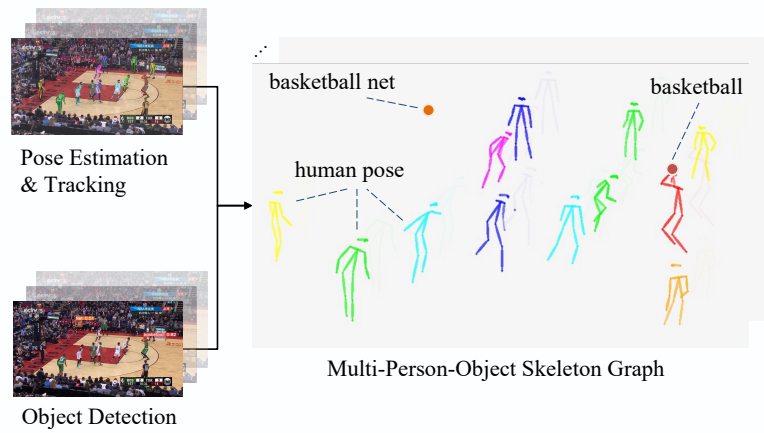


Fig. 1: A group activity is represented as a panoramic graph which consists of multi-person skeletons and object keypoints.

bounding boxes and model interactions between actors using RNNs, GNNs, or Transformers. Recognizing actions from RGB data can be challenging due to background variations, motion blurs and occlusions [56]. Furthermore, RGB videos often contain redundant information and are large in data size. In group activity scenarios, high resolution and frame rate are crucial for accurate detection and recognition. However, most RGB-based methods have to reduce the batch size [70] or employ frame sampling [20, 28] to manage the high computational and memory demands. These compromises significantly constrain the application of RGB-based GAR methods.

To overcome the shortcomings of RGB-based methods, several recent approaches [18, 34, 41, 58, 73] have attempted to leverage human pose for group activity recognition. These approaches extract keypoints using pose estimation backbones and take keypoints either as the sole input [41, 58, 73] or as a supplement to RGB inputs [18, 34]. However, these methods lack effective structural prior for the relationships of keypoints, thus requiring relational reasoning among them [41], or specialized hierarchical models to incrementally aggregate from keypoints to group-level features [73]. Furthermore, they rely on ground-truth individual bounding boxes and ball annotations for accurate localization and tracking before recognition.

Considering joints as nodes and bones as edges, the human pose can naturally construct a skeletal graph. This topology provides a strong prior, enhancing the feature extraction capabilities of spatial and temporal graph convolutions [68]. Consequently, Graph Convolutional Networks (GCNs) have achieved great success in skeleton-based action recognition [9, 50, 53, 68]. However, existing approaches are primarily based on the single-person skeletal topology. When multiple participants are involved, these approaches typically divide the multi-person skeletal data into multiple single-person graphs and stack them

in the sample dimension. Under this processing, the weights of multiple people are shared within the network, resulting in the interactions between individuals being largely neglected [36, 74]. Moreover, the absence of object data in conventional skeleton datasets [38] leads to a significant loss of critical information related to objects.

To address the aforementioned shortcomings, we introduce a novel pipeline for skeleton-based GAR. This pipeline begins with the estimation of human poses from videos and the construction of a multi-person skeleton graph, followed by the recognition using a spatial-temporal graph convolution network. Initially, we employ pre-trained pose estimation and object detection methods [16, 26, 55] to extract keypoints for both humans and objects. Instead of relying on ground-truth tracklets, we develop a reassignment strategy coupled with pose tracking algorithms [1, 62] to enhance consistent identity assignments across frames. Subsequently, as illustrated in Fig. 1, we design a panoramic multi-person-object graph that integrates the keypoints of multiple human skeletons and objects. This panoramic graph overcomes the limitations of vanilla human skeleton representations, including the constrained single-person graph scale and the lack of object information. Lastly, we propose MP-GCN for skeleton-based GAR. Extensive experimental evaluations on Volleyball, NBA, and Kinetics demonstrate that the proposed method outperforms state-of-the-art keypoint-based methods. The contributions are summarized as follows:

- We develop a new pipeline for skeleton-based group activity recognition that does not require ground-truth individual boxes and labels. It includes acquiring keypoints through pose estimation and tracking algorithms and recognizing activities using skeleton-based graph convolutional network.
- We design a panoramic multi-person-object graph to represent group activity, which addresses the shortcomings of previous methods and unifies intra-person and inter-person interaction modeling.
- Using only estimated human pose and object keypoints, our method outperforms previous approaches on three widely used datasets with significantly lower computation cost compared to RGB-based methods.

2 Related Work

2.1 Group Activity Recognition

GAR [11] has been extensively studied due to its wide-ranging applications in the real world. The majority of the existing methods rely on RGB video either as the sole input modality or as the primary modality combined with optical flow and pose data. Early methods extracted hand-crafted features and utilized probabilistic graphical models [2, 5, 10, 31, 32, 47, 61] or AND-OR graphs [3, 4, 52] to infer group activities. RNN-based methods [7, 12, 24, 25, 35, 45, 51, 60, 65] were proposed due to RNN’s capability for temporal modeling. Hierarchical LSTM models [25, 51, 60] were also proposed to capture spatial-temporal dependencies.

Interaction modeling has attracted considerable attention in GAR. Researchers commonly employ interaction graphs [6, 12, 15, 23, 45, 63, 67, 70] to depict the relationships between actors. Typically, they extract features using a CNN backbone with individual bounding boxes and learn interactions from the relation graph through RNNs [12, 45], GCNs [63], GATs [15], or more customized modules such as a dynamic inference network [70] or a cross inference block [67]. Recently, transformer-based methods [18, 28, 34, 40, 43, 44, 73, 75] are predominant in GAR. These methods exploit attention mechanisms to model spatio-temporal relationship between individuals [20, 40, 43] or sub-groups [34, 73], integrating local information into group-level tokens for activity classification.

Skeleton-based GAR. Video-based methods for GAR often require substantial computational resources and encounter issues such as background variations and camera settings. As a result, several studies [13, 14, 41, 58, 73] explore using pose as the only input. Perez *et al.* [41] propose a model for interaction reasoning between human skeleton joints and ball keypoints. Duan *et al.* [14] generate heatmap volumes using estimated 2D pose data from videos and feed them into 3D CNN for action recognition. Zhou *et al.* [73] develop a multi-scale transformer that hierarchically accumulates group tokens from original joint information. Another study by Duan *et al.* [13] captures short individual skeleton sequence using graph convolutions and models inter-sequence interactions using Transformer encoders in general action recognition tasks. In contrast to the aforementioned work, we introduce a multi-person-object graph to represent group activities and employ GCN to perform global graph convolution directly.

2.2 GCN for Skeleton-based Action Recognition

Spatial Temporal GCNs [9, 39, 50, 53, 68] are widely adopted for modeling skeleton sequences in action recognition. They represent the movements of an individual as a spatial-temporal graph and perform the spatial-temporal graph convolution following [30, 68]. However, these models face scalability issues when applied to multi-person scenarios. Conventional GCN methods split skeletons of multiple people, perform graph convolutions with shared weights, and average these single-person features to form a collective group representation for classification.

Skeleton-based Human Interaction Recognition. Several GCN-based methods have attempted to model the interactive relations for recognition [17, 36, 74]. Zhu *et al.* [74] adopt inter-body graph convolution with a dynamic relational adjacency matrix, executed alongside the single-person graph convolution. Li *et al.* [36] address the scalability issues of conventional GCN by applying graph convolution to a two-person graph that simultaneously encompasses inter-body and intra-body joint relationships. Inspired by these innovations, our method constructs a multi-person graph that depicts the interactions among all participants and objects in group activities.

Skeleton Representation with Object. Some work integrates object information to enhance skeleton-based action recognition [29, 64]. In contrast, our study focuses on introducing keypoint information in group activities.

To address the limitations in video and conventional skeleton representation, we propose a multi-person-object graph, which provides a panoramic view to depict all the individuals and objects involved in a group activity sequence.

3 Method

3.1 Preliminaries

Human Skeleton Representation. The skeleton representation uses N joints and several bones to denote a person’s body. In each frame, one body can be represented as a spatial graph $\mathcal{G} = (\mathcal{V}, \mathcal{E}, \mathcal{X})$, where $\mathcal{V} = \{v_i | i = 1, \dots, N\}$ is the vertex set of N joints, and $\mathcal{E} = \{e_{ij} | i, j = 1, \dots, N\}$ is the edge set. An undirected edge $e_{ij} \in \mathcal{E}$ represents the bone connection between v_i and v_j . The relational adjacency matrix $\mathbf{A} \in \mathbb{R}^{N \times N}$ denotes all edges with its element a_{ij} representing the strength of e_{ij} . $\mathcal{X} \in \mathbb{R}^{T \times N \times C}$ is the C -channel feature map of a sequence in T frames, typically the 2D/3D joint coordinates.

Graph Convolution. Most GCN-based methods follow a similar paradigm. The backbone of these methods typically consists of several basic blocks. Each basic block is composed of a Spatial Graph Convolution (SGC) layer and a Temporal Convolution Network (TCN) layer, which captures the spatial relationships among skeleton joints within a single frame and the temporal dependencies across multiple frames, respectively. Yan *et al.* [68] describe the SGC operation as

$$f_{\text{out}}(v_i) = \sum_{v_j \in B(v_i)} \frac{1}{Z_i(v_j)} f_{\text{in}}(v_j) \cdot \mathbf{w}(l_i(v_j)), \quad (1)$$

where $f_{\text{in}}()$ and $f_{\text{out}}()$ are input and output features of the corresponding joints, respectively. The node v_i denotes the i -th joint, with $B(v_i)$ representing its neighbor set. The labeling function $l_i : B(v_i) \rightarrow \{0, \dots, K - 1\}$ assigns each neighbor node to one of K subsets. That weight function \mathbf{w} is applied to the categorized neighbor nodes, and $Z_i(v_j)$ serves as a normalizing term to balance the influence of different subsets.

3.2 Panoramic Graph Convolution

Human-Object Graph. For scenes involving multiple people, an activity sequence is represented by $\mathcal{X} \in \mathbb{R}^{T \times M \times N \times C}$, where M is the number of participants. This skeleton representation only includes the coordinates of the human body, thus it often suffers from the absence of object information [38]. To address this issue, we introduce keypoints to represent objects and integrate them with human pose to form a human-object graph. The skeletal sequence is expanded to $\mathcal{X} \in \mathbb{R}^{T \times M \times N' \times C}$, where $N' = (N + n)$. Notably, the number of objects keypoints n and how they connect with human skeletons can be arbitrarily defined. In this paper, we introduce the ball as one point corresponding to the center of its bounding box and empirically connect it with both hands.

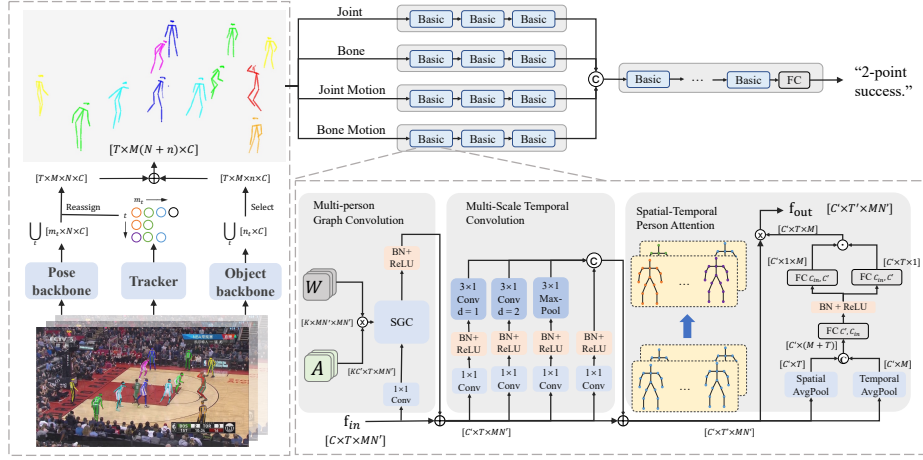


Fig. 2: Architecture of MP-GCN and components of the basic block, where C, C', T, T', N' and K denote the numbers of input channels, output channels, input frames, output frames, joints, and subsets in SGC, respectively. \odot , \otimes , and \oplus represent the matrix production, element-wise production, and concatenation, respectively.

Multi-Person Graph. In contrast to prior work [9, 39, 50, 68] that process multiple skeletons by separating them and batching them in the sample domain, our approach views all individuals in a scene as a unified group. Given an activity involving M participants, we organize the activity sequence as a multi-person graph $\mathcal{X} \in \mathbb{R}^{T \times MN \times C}$ with an adjacency matrix $\mathbf{A} \in \mathbb{R}^{MN \times MN}$. \mathbf{A} is partitioned into blocks $\mathbf{A}_{ij} \in \mathbb{R}^{N \times N}$. Specifically,

$$\mathbf{A} = \begin{bmatrix} \mathbf{A}_{11} & \mathbf{A}_{12} & \cdots & \mathbf{A}_{1M} \\ \mathbf{A}_{21} & \mathbf{A}_{22} & \cdots & \mathbf{A}_{2M} \\ \vdots & \vdots & \ddots & \vdots \\ \mathbf{A}_{M1} & \mathbf{A}_{M2} & \cdots & \mathbf{A}_{MM} \end{bmatrix} \quad (2)$$

where the diagonal blocks \mathbf{A}_{ii} capture the intra-body connections for each individual i , while the off-diagonal blocks represent inter-body relationships. To construct this graph, we define the natural body topology as the intra-body graph and introduce pairwise inter-body links. These links connect the central body joints and object keypoints for every pair of individuals. Afterwards, we create a panoramic multi-person-object graph by integrating the concepts of human-object and multi-person graphs. This graph consists of spatial-temporal features $\mathcal{X} \in \mathbb{R}^{T \times MN' \times C}$ with an expanded adjacency matrix $\mathbf{A} \in \mathbb{R}^{MN' \times MN'}$. Compared to scene graphs that reduce each identity to a single node or the conventional single-person skeletons, the proposed panoramic graph provides a more detailed and holistic representation of the group activity.

Spatial Graph Convolution. The graph convolution operation is applied to extract information embedded in the multi-person-object skeleton graph. When

implemented with adjacency matrix \mathbf{A} , Eq. (1) can be articulated as

$$\mathbf{f}_{out} = \sum_{k=0}^{K-1} \Lambda_k^{-\frac{1}{2}} \mathbf{A}_k \Lambda_k^{-\frac{1}{2}} \mathbf{f}_{in} \mathbf{W}_k \quad (3)$$

In this paper, we maintain the maximum graph sampling distance D to 1 and set the number of subsets K to 3 as in [68]. We design an intra-inter partitioning strategy to accommodate multi-person graph structure. In Eq. (3), \mathbf{f}_{in} and \mathbf{f}_{out} denote the input and output feature maps. The matrices \mathbf{A}_0 , \mathbf{A}_1 and \mathbf{A}_2 correspond to self links, intra-person connections and inter-person connections, respectively. Λ_k is used to normalize \mathbf{A}_k , and the learnable parameter \mathbf{W}_k represents the edge importance weighting. This partitioning strategy allows GCN to capture both intra-person and inter-person interactions through a singular graph convolution framework.

3.3 Model Architecture

Building on the multi-person spatial graph convolution, we propose MP-GCN for skeleton-based GAR, as illustrated in Fig. 2. Current state-of-the-art methods [9, 18, 34, 50] often employ a multi-stream architecture and fuse the prediction scores at the final stage. Such ensemble techniques like late-fusion are beneficial for improving model performance, but they linearly increase model complexity with the addition of input modalities. Instead, we incorporate ideas from [18, 39, 53] to construct an early-fusion network. Our MP-GCN contains four input branches and a main branch. Each input branch contains several basic blocks to extract low-level features from one of four aspects of skeletal data: joint, bone, joint motion, and bone motion (detailed preprocessing steps are provided in the Appendix). Subsequently, we concatenate the feature maps from the four streams into the main branch at an early stage. The main branch continues with additional basic blocks and classification head. This architecture retains rich information from different inputs but significantly reduces complexity compared to conventional ensemble solutions.

Basic Block. The basic block consists of an SGC, Multi-Scale TCN, and Spatial-Temporal Person Attention block with module-wise residual links. In the SGC, graph convolution is performed on the entire panoramic graph, maintaining the graph scale throughout the network. For the TCN, we propose a four-branch multi-scale temporal convolution layer following [39] to capture temporal dynamics in consecutive frames. Each branch contains a bottleneck layer for channel transformation, BatchNorm and ReLU, and ends with 3×1 convolutional layers with specified dilation in the first two branches and a Max-Pooling layer in the third branch.

Spatial-Temporal Person Attention. A group activity is often characterized by key roles that can vary rapidly over time [40]. To capture the key individuals throughout an activity, we design a Spatial-Temporal Person Attention Module, based on [54]. It computes attention scores for M people across T frames. It starts by averaging the feature maps in person and frame dimensions. Then, it

concatenates the averaged features into a $C \times (M + T)$ vector. Subsequently, two convolutional layers are designed to derive person-wise and frame-wise scores, which are multiplied to generate the final spatial-temporal attention map. This attention module enables MP-GCN to focus on key individuals and objects in crowded scenes and to mitigate the impact of irrelevant roles.

3.4 Tracking-based Pose Reassignment

Despite the widespread application of motion capture and ball tracking systems in sports analysis [21], there are few publicly available datasets for skeleton-based GAR. Therefore, we extract 2D skeleton coordinates from original RGB videos using pre-trained pose estimators and object detectors [16, 26, 55].

Human Pose Tracking have proven to be vital for action recognition [13, 46], yet their adoption for associating skeleton data in the respective of recognition remains limited. For a group activity sequence, the extracted human pose can be denoted as $\bigcup_t \mathcal{X}'_t$, where $\mathcal{X}'_t \in \mathbb{R}^{m_t \times N \times C}$ and the number of detected actors m_t may change along t . We leverage a ReID tracker that assigns unique IDs to the same person identified across frames. However, occlusions, miss detections and the identification of non-relevant individuals occur frequently. To enhance data consistency and filter out irrelevant individuals when preparing the skeletal data, we develop a pose assignment strategy which maps a variable number of individuals per frame to a fixed number M using $r : N^+ \rightarrow \{0, \dots, M - 1\}$.

Reassignment strategy. Assuming m_t people are detected in frame t , each person is assigned a track ID $id(m)$ and an associated detection confidence $conf(m)$. For the individual with index m , we define the sequence $S_{id(m)} = (x_t, y_t)_{t=1}^{t_{id(m)}}$ which represents the trajectory of person m 's center coordinates (x_t, y_t) over $t_{id(m)}$ frames identified by the same track ID $id(m)$. The activeness of a person with track ID $e(id(m))$ is evaluated using $e(id(m)) = \exp(s(id(m))) / \sum_{i=1}^{m_t} \exp(s(id(i)))$, where

$$s(id(m)) = \sqrt{\sum_{t=1}^{t_{id(m)}} \frac{(x_t - \bar{x})^2}{t_{id(m)}}} + \sqrt{\sum_{t=1}^{t_{id(m)}} \frac{(y_t - \bar{y})^2}{t_{id(m)}}} \quad (4)$$

In Eq. (4), $\bar{x} = 1/t_{id(m)} \sum_{t=1}^{t_{id(m)}} x_t$ and $\bar{y} = 1/t_{id(m)} \sum_{t=1}^{t_{id(m)}} y_t$. $s(id(m))$ signifies the standard deviation of the trajectory $S_{id(m)}$. The pose reassignment contains two stages. First, in each frame, it selects individuals with at most highest M scores, where the score is determined by $score(id(m)) = conf(m) + e(id(m))$. We map the chosen track IDs to a fixed range using $r(id(m)) = id(m) \bmod M$ for the first assignment. In case of a conflict, the person with smaller track ID will be assigned, while the others are reserved for the second assignment. Subsequently, the remaining individuals are allocated to the available indices in order. This reassignment strategy prioritizes who are more likely to play a significant role in group activities and enhance temporal consistency of the obtained skeletal data.

4 Experiments

4.1 Datasets

Volleyball Dataset [25] contains 4,830 clips from 55 volleyball game records. Each clip, consisting of 41 frames, is labeled with one of eight group activities. The authors also provide labels of individual actions (9 classes) and bounding boxes for every athlete in the central frame. For fully supervised studies, researchers commonly use the group activities, individual action labels, and the ground-truth person bounding box of the middle 20 frames [49]. We report the Multi-class Classification Accuracy (MCA) for group activity and the Mean Classification Accuracy of individual action (IMCA) on Volleyball Fully Supervised following most methods. In contrast, weakly supervised methods only utilize group-level activity labels. On Volleyball Weakly Supervised, we follow previous methods [28, 66] and report MCA and Merged-MCA (MMCA, which merges *left/right set* and *left/right pass* into *left/right pass-net*).

NBA Dataset. NBA [66] contains 9,172 clips (7,624 for training and 1,548 for testing) derived from 181 NBA game records. Each clip, composed of 72 frames, is labeled with one of nine basketball scoring activities. This is the largest dataset currently for group activity recognition, providing only the group-level activity annotations. For evaluation, we report the Multi-Class Accuracy (MCA) and Mean Per-Class Accuracy (MPCA), consistent with previous methods.

4.2 Implementation Details

Keypoint Acquisition. We adopt YOLOv8 [26] for pose estimation and object detection. We utilize YOLOv8x-pose with weights pre-trained on the COCO dataset [37] for pose estimation ($V=17$), and employ BoTSort [1] for multi-person tracking. For both the Volleyball and NBA datasets, we set the number of actors in each frame M to 12. Additionally, we fine-tune the pretrained YOLOv8x model on our custom dataset for detecting basketballs and basketball nets on the NBA dataset. This dataset includes 5,000 sample images manually annotated by us from the NBA dataset. Please refer to Appendix for details about the keypoint extraction process.

Hyper Parameters. We set the number of frames T to the original length of each clip, $T = 41$ for Volleyball Weakly Supervised and $T = 72$ for NBA dataset. In four input branches, the input-output channels for 3 basic blocks are 6-64, 64-64, 64-32. In the main branch, the channels for the 6 basic blocks are 128-128, 128-128, 128-128, 128-256, 256-256, 256-256. The training and testing batch size for both the Volleyball and NBA datasets is set to 16. We train our model for 65 epochs, employing a warm-up strategy [22] for the first 5 epochs to ensure stable training. The learning rate is initially set to 0.1 and decays according to a cosine scheduler after the 5th epoch. We use cross-entropy loss as the training objective and an SGD optimizer with Nesterov momentum of 0.9 and weight decay of 0.0002.

Table 1: Comparison with state-of-the-art methods on the Volleyball dataset. The best results are highlight in **bold**, and the second-best results are underlined.

Method	Keypoint RGB Flow			Backbone	Benchmark	
					MCA	IMCA
Fully Supervised					MCA	IMCA
ARG [63]		✓		VGG-19	92.6	82.6
HiGCIN [67]		✓		ResNet-18	91.4	-
DIN [70]		✓		VGG-16	93.6	-
GIRN [41]	✓			OpenPose	92.2	-
POGARS [58]	✓			Hourglass	93.9	-
COMPOSER [73]	✓			HRNet	94.6	-
SkeleTR [13]	✓			HRNet	94.4	-
MP-GCN (Ours)	✓			HRNet	95.5	84.6
CRM [6]		✓	✓	I3D	93.0	-
AT [18]	✓	✓		I3D+HRNet	93.5	85.7
SACRF [43]	✓	✓	✓	I3D+AlphaPose	95.0	83.1
GroupFormer [34]	✓	✓	✓	I3D+AlphaPose	95.7	85.6
Dual-AI [20]		✓	✓	Inception-v3	95.4	85.3
MP-GCN (Ours) + VGG16	✓	✓		HRNet+VGG16	96.2	-
Weakly Supervised					MCA	MMCA
SAM [66]		✓		ResNet-18	86.3	93.1
DFWSGAR [28]		✓		ResNet-18	90.5	94.4
Dual-AI [20]		✓	✓	Inception-v3	-	<u>95.8</u>
KRGFormer [40]		✓		Inception-v3	92.4	95.0
Tamura <i>et al.</i> [57]		✓		I3D+DETR	96.0	-
MP-GCN (Ours)	✓			YOLOV8x	<u>92.8</u>	96.1

4.3 Comparison with State of the Arts

Volleyball Dataset. The results are presented in Tab. 1. For a fair comparison, results for fully supervised settings (using groundtruth box) and for weakly supervised settings (using estimated detections) are listed separately. In the fully supervised setting, we utilize the skeletal data extracted by COMPOSER [73], which employs HRNet [55] with GT human bbox [49] ($T=20$). We report the results for previous RGB-based or multi-modal methods [6, 18, 20, 34, 43, 63, 67, 70] and results for keypoint-based methods [18, 41, 73] that rely solely on human pose and ball annotations [41]. With strong supervision provided by ground-truth individual bounding boxes for human pose tracking, our method achieves a remarkable result: 95.5% in MCA, outperforming both keypoint-based and RGB-based approaches. Meanwhile, our method can perform individual action recognition using single-person skeleton graph, obtaining 84.6% in IMCA. Moreover, we combine our model’s prediction with scores of VGG-16 backbone (which achieves 92.3% on Volleyball) and finally obtain 96.2% in MCA. This result demonstrates our method’s effectiveness in predicting the group activity from a complex scene and its further complementarity with RGB-based methods. In

Table 2: Comparison with state-of-the-art methods on the NBA dataset. * denotes that MCA and MPCA are reported in [28].

Method	Input	#Params	FLOPs	MCA	MPCA
*ARG [63]	RGB	45.4M	614.2G	59.0	56.8
*AT [18]	RGB	29.6M	609.9G	47.1	41.5
SAM [66]	RGB	-	-	49.1	47.5
*DIN [70]	RGB	28.6M	613.8G	61.6	56.0
dual-AI [20]	RGB	-	-	51.5	44.8
KRGFormer [40]	RGB	-	-	72.4	67.1
DFWSGAR [28]	RGB	17.4M	628.1G	75.8	71.2
MP-GCN (Ours, $T=18$)	kpt	4.4M	5.70G	73.3	68.4
MP-GCN (Ours, $T=72$)	kpt	4.4M	22.3G	<u>76.0</u>	<u>71.9</u>
MP-GCN (Ours, late-fusion)	kpt	11.6M	50.4G	78.7	74.6

the weakly supervised setting, ground-truth bounding boxes are replaced with estimated tracklets obtained using YOLOv8 [1, 26]. As shown in Tab. 1, our method outperforms others under both fully and weakly supervised settings. In the weakly supervised setting, our method still achieves satisfying results: 92.8% MCA and 96.1% MMCA. This result demonstrate our method’s compatibility to both high-quality and noisy keypoints data.

NBA Dataset. Table 2 presents the state-of-the-art comparison on the NBA dataset. The CNN backbone for RGB-based methods is set to ResNet-18 with an input resolution of 720×1280 and $T=18$ (except for [20], which uses Inception-v3 and $T=3/20$ for training/testing). We follow the same pose estimation implementation as in Volleyball Weakly Supervised and also detect balls and basketball nets using YOLOV8 [26]. Furthermore, for methods with available official implementation, we also report the model’s number of parameters and FLOPs in the recognition phase. Note that #Params and FLOPs of the backbone for RGB-based methods are included since the CNN backbone is tuned during training, whereas the computational cost of our pose backbone is only considered for skeleton dataset acquisition and is not included. Our method outperforms video-based methods in MCA with significantly fewer parameters and lower computational costs. When late-fusion is adopted, our method significantly surpasses video-based methods. Please refer to Appendix for a detailed comparison between keypoint-based methods [9, 33, 39, 68] in terms of accuracy, computational cost and backbone efficiency.

4.4 Ablation Study

Graph Structure. Suppose P denotes the number of graphs for each sequence and N denotes the number of points in a graph. To validate the proposed multi-person graph, we experiment with the following graph settings on the Volleyball dataset. (1) Baseline: each sample is represented by M weight-shared graphs of V nodes. (2) Baseline with non-shared weights: M single-person graphs with

Table 3: Comparison of different graph structures in number of parameters, FLOPs and MCA (%) on Volleyball Fully Supervised.

Graph Structure	P	N	#Param.	FLOPs	MCA
Baseline	12	V	1.47M	2.21G	93.66
Baseline (non-shared weights)	12	V	1.78M	2.21G	94.54
Panoramic (only intra links)	1	$12V$	3.70M	4.19G	95.21
Panoramic (intra+inter links)	1	$12V$	3.70M	4.19G	95.54

Table 4: Comparison of different M in MCA (%) on the NBA dataset.

M	MCA
3	71.71
6	73.45
9	74.61
12 (Ours)	75.96
15	74.49

Graph Structure	N	MCA
pose	V	65.83
pose* M	$12V$	69.21
pose* M + ball	$12V+1$	69.51
pose* M + ball + net	$12V+2$	73.06
(pose-ball)* M	$12(V+1)$	72.94
(pose-ball-net)* M (Ours)	$12(V+2)$	75.96

non-shared weights. (3) Panoramic intra-person graph: a multi-person graph with only intra-person edges. (4) Panoramic graph: a multi-person-object graph with both intra- and inter-person connections. As presented in Tab. 3, using the multi-person graph scale results in a significant improvement of about 1.5% with tolerable increases in parameters and FLOPs. These results demonstrate the effectiveness the panoramic graph structure. Additionally, Table 4 presents an ablation study of M on the NBA dataset and demonstrate that $M = 12$ obtains the highest accuracy. This finding is consistent with the typical composition of a basketball game, which involves 10 athletes and 2-3 referees. It also suggests that the proposed reassignment strategy effectively maintains the key roles on the court.

Effect of Object. To further investigate the effect of object information, we examined graph structures incorporating objects in various configurations, as presented in Tab. 3. $\text{pose}^*M + \{\text{ball}/+\text{net}\}$ consists of $MV + v$ nodes, including M people and v object points (ball/+basketball net) connected to the hands of each actor. $(\text{pose}-\{\text{ball}/+\text{net}\})^*M$ introduces individual object nodes for each person, which are initialized with the same data. Placing the object keypoints separately from the multi-person skeletons leads to significantly lower accuracy compared to having individual non-shared object keypoints. Additionally, the inclusion of extra objects, such as the basketball net, further enhances recognition accuracy, indicating the effectiveness and generalizability of the proposed panoramic graph.

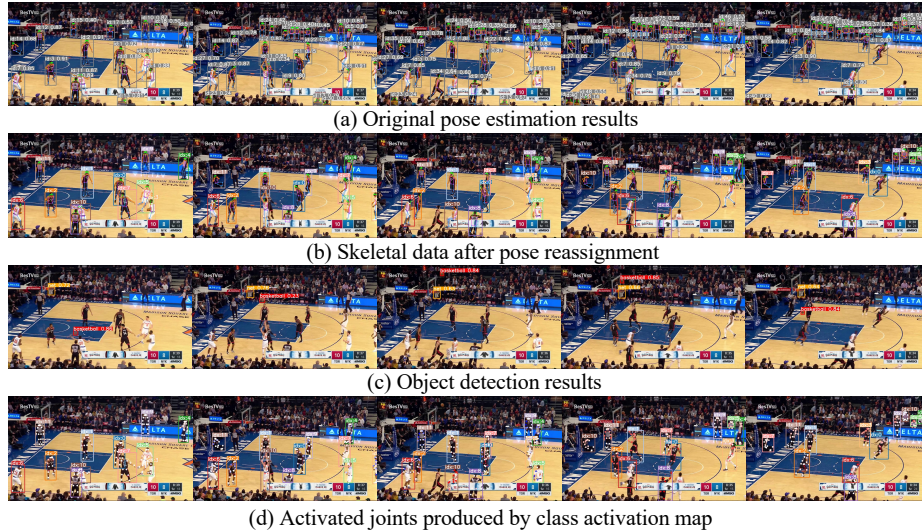


Fig. 3: Visualization of the extracted skeletons, object keypoints and activation maps.

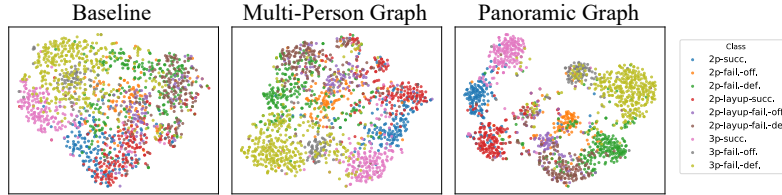


Fig. 4: *t*-SNE feature embedding visualization on NBA dataset for different graphs.

4.5 Visualization

Visualization of Keypoints and Activation Maps. In Fig. 3, we visualize the human skeletons and object keypoints for a 5-frame clip from the NBA dataset. In Fig. 3 (a)-(b), it is evident that the proposed reassignment strategy effectively selects athletes and referees from a multitude of detected candidates. However, when the number of people in the scene is insufficient, it inevitably includes unrelated individuals off the court. In Fig. 3 (c), our method effectively detects fast-moving basketballs. In addition, we visualize the class activation map [72] of this sequence in Fig. 3 (d). Our model correctly focuses on the shooter and referee when the shooter attempts a two-point shot.

Visualization of Embedding Feature. Figure 4 presents the *t*-SNE [59] visualization of different graph structures. It is evident that the proposed multi-person-object graph facilitates a clear separation of each class, while also producing a reasonable distribution of similar classes. For instance, the "2-point-layup-failed-offensive-rebound" and "2-point-layup-failed-defensive-rebound" samples are closely located in the embedding space.

Table 6: SOTA Comparison of keypoint-based methods on Kinetics400 dataset.

Method	Pose Estimator	Acc.
ST-GCN [68]		30.7
AGCN [50]	OpenPose [8]	36.1
MS-G3D [39]		38.0
Hachiuma <i>et al.</i> [19]	PPNv2 [48]	43.1
Hachiuma <i>et al.</i> with objects [19]		52.3
MS-G3D [39]		45.1
PoseConv3D($\mathbf{J}+\mathbf{B}$) [14]	HRNet [55]	47.7
Hachiuma <i>et al.</i> [19]		50.3
MP-GCN(Ours)	HRNet [55]	48.4
MP-GCN(Ours, late-fusion)		<u>51.1</u>

4.6 Towards in-the-wild Skeleton-based Action Recognition

To validate the generalization of our method, we also tested it on the Kinetics400 dataset [27], which has over 300k videos across 400 action classes, presenting significant challenges for skeleton-based action recognition. We use the same skeletal data provided by Duan *et al.* [14] and observe that 90% of the samples contain fewer than 4 individuals on average. Thus, we set M to 4 and keep other parameters unchanged. Table 6 presents the comparison between skeleton-based methods. It’s noticed that our method also achieves the remarkable accuracy on this daily living dataset. Notably, the introduction of object keypoints by Hachiuma *et al.* [19] substantially enhances recognition accuracy. This finding underscores the value of object information and suggests that the performance could be significantly improved by integrating object keypoints.

While our method has shown promising results, it is important to acknowledge that the performance of skeleton-based methods fall short of SOTA video-based methods [42], which obtain over 90% of accuracy on Kinetics400. This gap highlights the potential for future research to focus on enhancing multi-person and object representations, particularly in uncontrolled environments.

5 Conclusion

This paper proposes a new pipeline for Skeleton-based Group Activity Recognition. This pipeline includes human and object keypoints estimation, tracking-based pose reassignment, and collective activity recognition through panoramic graph convolutional network. The panoramic graph incorporates human pose and object keypoints into a multi-person-object skeleton graph, addressing the limitations of traditional human skeleton representation in shared weight, lack of inter-person interaction modeling, and absence of object information. Using skeletal data as the only input, the proposed method achieves state-of-the-art performance on three widely-used datasets (Volleyball, NBA, and Kinetics).

Acknowledgements

This work was supported by National Natural Science Foundation of China (grant No. 62376068, grant No. 62350710797), by Guangdong Basic and Applied Basic Research Foundation (grant No. 2023B1515120065), by Guangdong S&T programme (grant No. 2023A0505050109), by Shenzhen Science and Technology Innovation Program (grant No. JCYJ20220818102414031).

References

1. Aharon, N., Orfaig, R., Bobrovsky, B.Z.: Bot-sort: Robust associations multi-pedestrian tracking. arXiv:2206.14651 (2022)
2. Amer, M.R., Todorovic, S.: Sum product networks for activity recognition. *IEEE TPAMI* **38**(4), 800–813 (2016)
3. Amer, M.R., Todorovic, S., Fern, A., Zhu, S.C.: Monte carlo tree search for scheduling activity recognition. In: *ICCV*. pp. 1353–1360 (2013)
4. Amer, M.R., Xie, D., Zhao, M., Todorovic, S., Zhu, S.C.: Cost-sensitive top-down/bottom-up inference for multiscale activity recognition. In: *ECCV*. pp. 187–200 (2012)
5. Amer, M.R., Lei, P., Todorovic, S.: Hirf: Hierarchical random field for collective activity recognition in videos. In: *ECCV*. pp. 572–585 (2014)
6. Azar, S.M., Atigh, M.G., Nickabadi, A., Alahi, A.: Convolutional relational machine for group activity recognition. In: *CVPR*. pp. 7884–7893 (2019)
7. Bagautdinov, T., Alahi, A., Fleuret, F., Fua, P., Savarese, S.: Social scene understanding: End-to-end multi-person action localization and collective activity recognition. In: *CVPR*. pp. 3425–3434 (2017)
8. Cao, Z., Hidalgo, G., Simon, T., Wei, S.E., Sheikh, Y.: Openpose: Realtime multi-person 2d pose estimation using part affinity fields. *IEEE TPAMI* **43**(1), 172–186 (2021)
9. Chen, Y., Zhang, Z., Yuan, C., Li, B., Deng, Y., Hu, W.: Channel-wise topology refinement graph convolution for skeleton-based action recognition. In: *ICCV*. pp. 13339–13348 (2021)
10. Choi, W., Savarese, S.: A unified framework for multi-target tracking and collective activity recognition. In: *ECCV*. pp. 215–230 (2012)
11. Choi, W., Shahid, K., Savarese, S.: What are they doing? : Collective activity classification using spatio-temporal relationship among people. In: *ICCVW*. pp. 1282–1289 (2009)
12. Deng, Z., Vahdat, A., Hu, H., Mori, G.: Structure inference machines: Recurrent neural networks for analyzing relations in group activity recognition. In: *CVPR*. pp. 4772–4781 (2016)
13. Duan, H., Xu, M., Shuai, B., Modolo, D., Tu, Z., Tighe, J., Bergamo, A.: Skeletr: Towards skeleton-based action recognition in the wild. In: *ICCV*. pp. 13588–13598 (2023)
14. Duan, H., Zhao, Y., Chen, K., Lin, D., Dai, B.: Revisiting skeleton-based action recognition. In: *CVPR*. pp. 2959–2968 (2022)
15. Ehsanpour, M., Abedin, A., Saleh, F., Shi, J., Reid, I., Rezatofghi, H.: Joint learning of social groups, individuals action and sub-group activities in videos. In: *ECCV*. pp. 177–195 (2020)



16. Fang, H.S., Li, J., Tang, H., Xu, C., Zhu, H., Xiu, Y., Li, Y.L., Lu, C.: Alphapose: Whole-body regional multi-person pose estimation and tracking in real-time. *IEEE TPAMI* **45**(6), 7157–7173 (2023)
17. Gao, F., Xia, H., Tang, Z.: Attention interactive graph convolutional network for skeleton-based human interaction recognition. In: ICME. pp. 1–6 (2022)
18. Gavriluk, K., Sanford, R., Javan, M., Snoek, C.G.M.: Actor-transformers for group activity recognition. In: CVPR. pp. 836–845 (2020)
19. Hachiuma, R., Sato, F., Sekii, T.: Unified keypoint-based action recognition framework via structured keypoint pooling. In: CVPR. pp. 22962–22971 (2023)
20. Han, M., Zhang, D.J., Wang, Y., Yan, R., Yao, L., Chang, X., Qiao, Y.: Dual-ai: Dual-path actor interaction learning for group activity recognition. In: CVPR. pp. 2990–2999 (2022)
21. hawkeyeinnovations: Nba and sony’s hawk-eye innovations launch strategic partnership powering next generation tracking technology. <https://pr.nba.com/nba-sony-hawk-eye-innovations-partnership/> (2023)
22. He, K., Zhang, X., Ren, S., Sun, J.: Deep residual learning for image recognition. In: CVPR. pp. 770–778 (2016)
23. Hu, G., Cui, B., He, Y., Yu, S.: Progressive relation learning for group activity recognition. In: CVPR. pp. 977–986 (2020)
24. Ibrahim, M., Mori, G.: Hierarchical relational networks for group activity recognition and retrieval. In: ECCV. pp. 721–736 (2018)
25. Ibrahim, M.S., Muralidharan, S., Deng, Z., Vahdat, A., Mori, G.: A hierarchical deep temporal model for group activity recognition. In: CVPR. pp. 1971–1980 (2016)
26. Jocher, G., Chaurasia, A., Qiu, J.: Yolo by ultralytics (2023)
27. Kay, W., Carreira, J., Simonyan, K., Zhang, B., Hillier, C., Vijayanarasimhan, S., Viola, F., Green, T., Back, T., Natsev, P., Suleyman, M., Zisserman, A.: The kinetics human action video dataset. arXiv:1705.06950 (2017)
28. Kim, D., Lee, J., Cho, M., Kwak, S.: Detector-free weakly supervised group activity recognition. In: CVPR (2022)
29. Kim, S., Yun, K., Park, J., Choi, J.Y.: Skeleton-based action recognition of people handling objects. In: WACV. pp. 61–70 (2019)
30. Kipf, T.N., Welling, M.: Semi-supervised classification with graph convolutional networks. arXiv:1609.02907 (2017)
31. Lan, T., Sigal, L., Mori, G.: Social roles in hierarchical models for human activity recognition. In: CVPR. pp. 1354–1361 (2012)
32. Lan, T., Wang, Y., Yang, W., Robinovitch, S.N., Mori, G.: Discriminative latent models for recognizing contextual group activities. *IEEE TPAMI* **34**(8), 1549–1562 (2012)
33. Lee, J., Lee, M., Lee, D., Lee, S.: Hierarchically decomposed graph convolutional networks for skeleton-based action recognition. In: ICCV. pp. 10444–10453 (2023)
34. Li, S., Cao, Q., Liu, L., Yang, K., Liu, S., Hou, J., Yi, S.: Groupformer: Group activity recognition with clustered spatial-temporal transformer. In: ICCV. pp. 13648–13657 (2021)
35. Li, X., Chuah, M.C.: Sbgar: Semantics based group activity recognition. In: ICCV. pp. 2895–2904 (2017)
36. Li, Z., Li, Y., Tang, L., Zhang, T., Su, J.: Two-person graph convolutional network for skeleton-based human interaction recognition. *IEEE TCSVT* **33**(7), 3333–3342 (2023)

37. Lin, T.Y., Maire, M., Belongie, S., Hays, J., Perona, P., Ramanan, D., Dollár, P., Zitnick, C.L.: Microsoft coco: Common objects in context. In: ECCV. pp. 740–755 (2014)
38. Liu, J., Shahrourdy, A., Perez, M., Wang, G., Duan, L.Y., Kot, A.C.: Ntu rgb+d 120: A large-scale benchmark for 3d human activity understanding. *IEEE TPAMI* **42**(10), 2684–2701 (2020)
39. Liu, Z., Zhang, H., Chen, Z., Wang, Z., Ouyang, W.: Disentangling and unifying graph convolutions for skeleton-based action recognition. In: CVPR. pp. 140–149 (2020)
40. Pei, D., Huang, D., Kong, L., Wang, Y.: Key role guided transformer for group activity recognition. *IEEE TCSVT* **33**(12), 7803–7818 (2023)
41. Perez, M., Liu, J., Kot, A.C.: Skeleton-based relational reasoning for group activity analysis. *PR* **122**, 108360 (2022)
42. Piergiovanni, A.J., Kuo, W., Angelova, A.: Rethinking video vits: Sparse video tubes for joint image and video learning. In: CVPR. pp. 2214–2224 (2023)
43. Pramono, R.R.A., Chen, Y.T., Fang, W.H.: Empowering relational network by self-attention augmented conditional random fields for group activity recognition. In: ECCV. pp. 71–90 (2020)
44. Pramono, R.R.A., Fang, W.H., Chen, Y.T.: Relational reasoning for group activity recognition via self-attention augmented conditional random field. *IEEE TIP* **30**, 8184–8199 (2021)
45. Qi, M., Qin, J., Li, A., Wang, Y., Luo, J., Van Gool, L.: stagnet: An attentive semantic rnn for group activity recognition. In: ECCV. pp. 104–120 (2018)
46. Rajasegaran, J., Pavlakos, G., Kanazawa, A., Feichtenhofer, C., Malik, J.: On the benefits of 3d pose and tracking for human action recognition. In: CVPR (2023)
47. Ryoo, M.S., Aggarwal, J.K.: Stochastic representation and recognition of high-level group activities. *IJCV* **93**(2), 183–200 (2011)
48. Sekii, T.: Pose proposal networks. In: ECCV. pp. 342–357 (2018)
49. Sendo, K., Ukita, N.: Heatmapping of people involved in group activities. In: MVA. pp. 1–6 (2019)
50. Shi, L., Zhang, Y., Cheng, J., Lu, H.: Two-stream adaptive graph convolutional networks for skeleton-based action recognition. In: CVPR. pp. 12018–12027 (2019)
51. Shu, T., Todorovic, S., Zhu, S.C.: Cern: Confidence-energy recurrent network for group activity recognition. In: CVPR. pp. 4255–4263 (2017)
52. Shu, T., Xie, D., Rothrock, B., Todorovic, S., Chun Zhu, S.: Joint inference of groups, events and human roles in aerial videos. In: CVPR. pp. 4576–4584 (2015)
53. Song, Y.F., Zhang, Z., Shan, C., Wang, L.: Stronger, faster and more explainable: A graph convolutional baseline for skeleton-based action recognition. pp. 1625–1633 (2020)
54. Song, Y.F., Zhang, Z., Shan, C., Wang, L.: Constructing stronger and faster baselines for skeleton-based action recognition. *IEEE TPAMI* **45**(2), 1474–1488 (2023)
55. Sun, K., Xiao, B., Liu, D., Wang, J.: Deep high-resolution representation learning for human pose estimation. In: CVPR. pp. 5686–5696 (2019)
56. Sun, Z., Ke, Q., Rahmani, H., Bennamoun, M., Wang, G., Liu, J.: Human action recognition from various data modalities: A review. *IEEE TPAMI* **45**(3), 3200–3225 (2023)
57. Tamura, M., Vishwakarma, R., Vennelakanti, R.: Hunting group clues with transformers for social group activity recognition. In: ECCV. pp. 19–35 (2022)
58. Thilakarathne, H., Nibali, A., He, Z., Morgan, S.: Pose is all you need: The pose only group activity recognition system (pogars). *MVA* **33**(6), 95 (2022)

59. Van der Maaten, L., Hinton, G.: Visualizing data using t-sne. *JMLR* **9**(11) (2008)
60. Wang, M., Ni, B., Yang, X.: Recurrent modeling of interaction context for collective activity recognition. In: *CVPR*. pp. 7408–7416 (2017)
61. Wang, Z., Shi, Q., Shen, C., van den Hengel, A.: Bilinear programming for human activity recognition with unknown mrf graphs. In: *CVPR*. pp. 1690–1697 (2013)
62. Wang, Z., Zheng, L., Liu, Y., Li, Y., Wang, S.: Towards real-time multi-object tracking. In: *ECCV*. pp. 107–122 (2020)
63. Wu, J., Wang, L., Wang, L., Guo, J., Wu, G.: Learning actor relation graphs for group activity recognition. In: *CVPR*. pp. 9956–9966 (2019)
64. Xu, L., Lan, C., Zeng, W., Lu, C.: Skeleton-based mutually assisted interacted object localization and human action recognition. *IEEE TMM* **25**, 4415–4425 (2023)
65. Yan, R., Tang, J., Shu, X., Li, Z., Tian, Q.: Participation-contributed temporal dynamic model for group activity recognition. In: *ACM MM*. pp. 1292–1300 (2018)
66. Yan, R., Xie, L., Tang, J., Shu, X., Tian, Q.: Social adaptive module for weakly-supervised group activity recognition. In: *ECCV*. pp. 208–224 (2020)
67. Yan, R., Xie, L., Tang, J., Shu, X., Tian, Q.: Higcin: Hierarchical graph-based cross inference network for group activity recognition. *IEEE TPAMI* **45**(6), 6955–6968 (2023)
68. Yan, S., Xiong, Y., Lin, D.: Spatial temporal graph convolutional networks for skeleton-based action recognition. In: *AAAI*. pp. 7444–7452 (2018)
69. Yuan, H., Ni, D.: Learning visual context for group activity recognition. In: *AAAI*. pp. 3261–3269 (2021)
70. Yuan, H., Ni, D., Wang, M.: Spatio-temporal dynamic inference network for group activity recognition. In: *ICCV*. pp. 7476–7485 (2021)
71. Zhang, Y., Sun, P., Jiang, Y., Yu, D., Weng, F., Yuan, Z., Luo, P., Liu, W., Wang, X.: Bytetrack: Multi-object tracking by associating every detection box. In: *ECCV*. pp. 1–21 (2022)
72. Zhou, B., Khosla, A., Lapedriza, A., Oliva, A., Torralba, A.: Learning deep features for discriminative localization. In: *CVPR*. pp. 2921–2929 (2016)
73. Zhou, H., Kadav, A., Shamsian, A., Geng, S., Lai, F., Zhao, L., Liu, T., Kapadia, M., Graf, H.P.: Composer: Compositional reasoning of group activity in videos with keypoint-only modality. In: *ECCV*. pp. 249–266 (2022)
74. Zhu, L., Wan, B., Li, C., Tian, G., Hou, Y., Yuan, K.: Dyadic relational graph convolutional networks for skeleton-based human interaction recognition. *PR* **115**, 107920 (2021)
75. Zhu, X., Zhou, Y., Wang, D., Ouyang, W., Su, R.: Mlst-former: Multi-level spatial-temporal transformer for group activity recognition. *IEEE TCSVT* **33**(7), 3383–3397 (2023)

Skeleton-based Group Activity Recognition via Spatial-Temporal Panoramic Graph

Supplementary Material

Zhengcen Li^{1,2}, Xinle Chang¹, Yueran Li¹, and Jingyong Su^{1,2}

¹ Harbin Institute of Technology, Shenzhen, 518055, China

² Peng Cheng Laboratory, 518055, China

{lizhengcen, changxinle, liyueran}@stu.hit.edu.cn
sujingyong@hit.edu.cn

This appendix is organized as follows:

- 1 Details of Keypoint Acquisition
 - 1.1 Pose Estimation and Tracking
 - 1.2 Reassignment Strategy
- 2 Data Pre-processing of Multiple Inputs
- 3 Detailed Comparison between Keypoint-based Methods
- 4 Additional Qualitative Results
- 5 Additional Ablation Studies

1 Details of Keypoint Acquisition

1.1 Pose Estimation and Tracking

We use the pre-trained YOLOv8x-pose model to estimate human skeletons for Volleyball Weakly Supervised and NBA datasets. Our approach follows the official implementation of YOLOv8³. The YOLOv8x-pose model conforms to the COCO keypoint layout, which represents a person with 17 keypoints: nose, left eye, right eye, left ear, right ear, left shoulder, right shoulder, left elbow, right elbow, left wrist, right wrist, left hip, right hip, left knee, right knee, left ankle and right ankle. Both the Volleyball and NBA datasets are processed with the maximum number of actors in a single frame $M = 12$. We maintain the original resolution of each video clip when feed into YOLOv8x, as the videos in both Volleyball and NBA datasets have resolutions of 1920×1080 and 1280×720 . For pose tracking, we utilize the integrated BoT-SORT [1] tracker with default YOLO tracker settings.

Figure 1 shows the visualization of the skeletal data used in our experiments. Figure 1a illustrates the skeletons extracted from the NBA dataset during instances of high-speed camera movement. Although most actors can still be captured, the tracking results are not entirely satisfactory. Figure 1b shows the

³ <https://docs.ultralytics.com/tasks/pose>

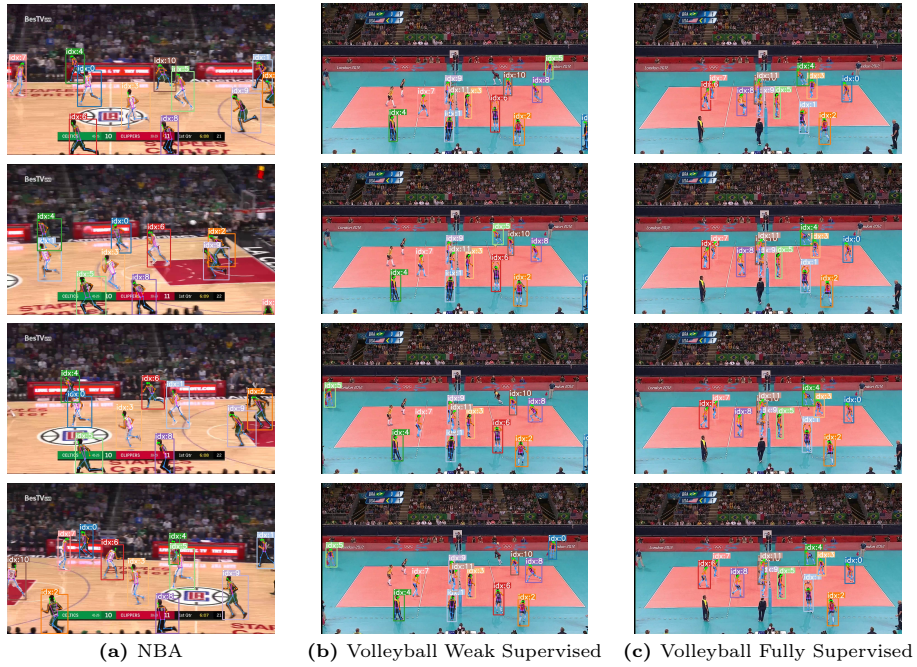


Fig. 1: The extracted skeletons of the Volleyball Fully Supervised (with GT bounding boxes), Volleyball Weakly Supervised, and NBA datasets.

results of extracting skeletons without using the ground truth individual detection. When compared with Fig. 1c which uses the ground truth boxes, errors in detecting and selecting key roles are more likely to occur.

In Figs. 2a and 2b, we illustrate the distribution of the number of individuals extracted in each frame from the Volleyball and NBA datasets. The number of individuals peaks at around 12 but frequently exceeds 20 in many frames. Figures 2c and 2d present the number of track IDs detected by the tracker in each clip, revealing that the majority of clips contain more than 12 track IDs. These findings underscore the necessity of adopting a reassignment strategy to accurately track important individuals across frames.

For the NBA dataset, the keypoints of basketball and basketball net are extracted using the YOLOv8x model. We initialize YOLOv8x with pre-trained weights and fine-tune for 50 epochs on the custom dataset. Figures 2e and 2f present the number of basketball nets and basketballs detected in each frame. It can be observed that basketballs and basketball nets are detected in approximately 75% of the frames and 90% of the frames, respectively.

Backbone Efficiency Comparison. Table 1 compares the FLOPs for RGB backbones used by prior works and YOLOv8x. The results indicate that YOLOv8x is more efficient than backbones such as VGG-16 and VGG-19. It should be noted that the task of skeleton-based action recognition only uses an off-the-shelf pose

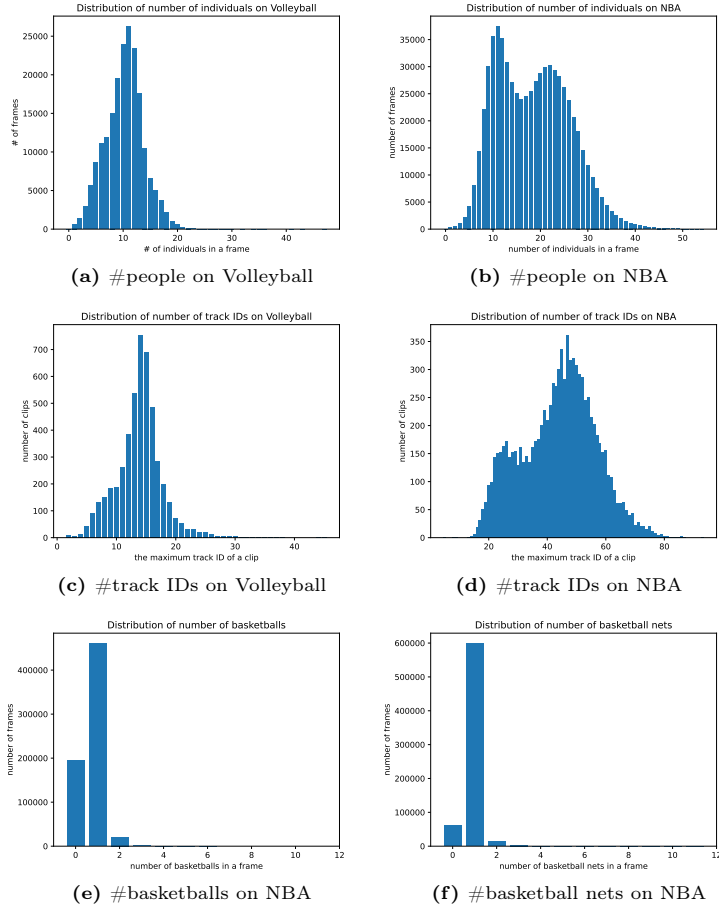


Fig. 2: The distribution of the number of detected people in each frame, the number of track IDs in each clip, and the number of detected objects in each frame.

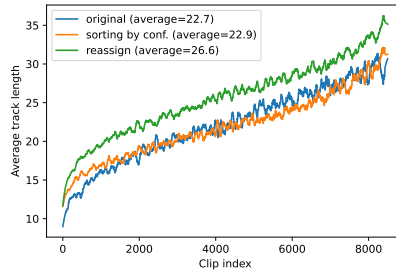


Fig. 3: Comparison of the averaged track length per clip for the estimated skeletons from NBA dataset using different processing strategies, including the original estimation, sorting by confidence, and our proposed reassignment strategy.

Table 1: Efficiency Comparison of RGB and pose backbones in FLOPs, $[T, H, W] = [1, 720, 1280]$.

YOLOv8x	VGG-16	VGG-19	Inception-v3	ResNet-18
258G	282G	358G	66G	33.7G

backbone for keypoint extraction, which occurs once during dataset preparation. In offline scenarios, the efficiency of the pose backbone is not a critical factor in the overall efficiency. Therefore, larger pose estimators are acceptable when producing skeleton data from a video dataset. For online usage, more efficient real-time pose estimators can be applied to reduce computational costs and latency.

1.2 Reassignment Strategy

As illustrated in Figs. 2b and 2d, for the NBA dataset, about 23 people are detected in each frame, while the tracker produces an average of 50 track IDs per clip. These results indicate that issues such as missed detection and lost tracks occur frequently. Therefore, we propose a reassignment strategy to mitigate the inconsistency issues.

In addition to the results presented in Tab. 2, we investigate the influence of different processing strategies on the average track length per video clip. Figure 3 compares the average tracking length per clip for the estimated skeletons from the NBA dataset using different processing strategies. These strategies include (1) the original estimation results, (2) selecting people with maximum confidences, and (3) the proposed reassignment strategy. The curve in Fig. 3 is produced by sorting by the mean track length of three strategies and smoothed using Savitzky–Golay filter. The reassignment strategy brings a steady improvement in the average tracking length (72 frames/clip) from 22.7 to 26.6 and brings $\sim 1.3\%$ improvement in accuracy compared to simply picking by maximum confidence.

Pose Estimation, Tracking and Reassignment. Table 2 summarizes the performance of our method using skeletons extracted by different methods [16, 55] which are widely used in skeleton-based action recognition [14, 34, 73]. The results indicate that our proposed reassignment strategy coupled with a tracking algorithm leads to a marked improvement in performance.

2 Data Pre-processing of Multiple Inputs

In this paper, we build upon previous studies in skeleton-based human action recognition [9, 39, 50, 54], developing four types of input features: 1) joint coordinates, 2) bone vectors, 3) joint motion features, and 4) bone motion features.

Suppose the original 2D/3D coordinates of a group activity sequence is $\mathcal{X} \in \mathbb{R}^{T \times MN \times C}$, where T , M , N , C denote the number of frames, number of people,

Table 2: Comparison of our method with only human skeleton data obtained by widely-used pose estimation and tracking algorithms in MCA (%) on NBA dataset

Pose Estimator	ReID Tracker	Reassign	MCA
HRNet [55]	no tracking		64.60
AlphaPose [16]	no tracking		64.92
	JDE [62]	✓	65.57
YOLOv8x [26]	no tracking		67.02
	BoT-SORT [1]		67.95
	BoT-SORT [1] (Ours)	✓	69.21

number of joints and input coordinates, respectively. For the Volleyball Fully Supervised, we adopt $C = 2$ to indicate the two-dimension keypoint coordinates. For the NBA and Volleyball Weakly Supervised datasets, we use $C = 3$ to represent the set $\{x, y, v\}$, where v denotes the visibility prediction from the pose backbone.

The input of joint coordinates is the concatenation of absolute locations \mathcal{X} and relative locations to the body center $\mathcal{X}_{relative}$, where

$$\mathcal{X}_{relative}[:, i, :] = \mathcal{X}[:, i, :] - \mathcal{X}[:, center_m, :], \quad (1)$$

$i = \{1, 2, \dots, MN\}$, and $center_m$ represents the index of the center joint of person m . The input of bone features is obtained by concatenating the bone vectors and their angles relative to the coordinate axes.

$$\begin{aligned} \mathcal{X}_{bone}[:, i, :] &= \mathcal{X}[:, i, :] - \mathcal{X}[:, i_{adj}, :], \\ \mathcal{X}_{angle}[:, i, c] &= \arccos \frac{\mathcal{X}_{bone}[:, i, c]}{\sqrt{\|\mathcal{X}_{bone}[:, i, :]\|^2}}. \end{aligned} \quad (2)$$

In Eq. (2), i_{adj} denotes the adjacent node of joint i , and $c = 1, 2$ denotes the 2D coordinates and $c = 1, 2, 3$ denotes the 3D coordinates.

Furthermore, the joint motion features are the concatenation of the motion X_{jm1} between consecutive frames and X_{jm2} two-hop frames.

$$\begin{aligned} \mathcal{X}_{jm1}[t, :, :] &= \mathcal{X}[t + 1, :, :] - \mathcal{X}[t, :, :], \\ \mathcal{X}_{jm2}[t, :, :] &= \mathcal{X}[t + 2, :, :] - \mathcal{X}[t, :, :]. \end{aligned} \quad (3)$$

In Eq. (3), $t = \{1, 2, \dots, T\}$. Similarly, the bone motion features are calculated by connecting the motion of bone features X_{bm1} and X_{bm2} .

$$\begin{aligned} \mathcal{X}_{bm1}[t, :, :] &= \mathcal{X}_{bone}[t + 1, :, :] - \mathcal{X}_{bone}[t, :, :], \\ \mathcal{X}_{bm2}[t, :, :] &= \mathcal{X}_{bone}[t + 2, :, :] - \mathcal{X}_{bone}[t, :, :]. \end{aligned} \quad (4)$$

Afterwards, these four features in $T \times MN \times 2C$ are feed into four separate input branches, respectively.

Table 3: Comparisons with state-of-the-art (SOTA) methods that leverage only keypoint information on the Volleyball Dataset.

Method	Pose Backbone	Pose	Object	Acc.
GIRN [41]	OpenPose	✓		88.4
		✓	✓	92.2
AT [18]	HRNet	✓		92.3
		✓	✓	92.8
POGARS [58]	Hourglass	✓		93.2
		✓	✓	93.9
COMPOSER [73]	HRNet	✓		93.7
		✓	✓	94.6
SkeleTR [13]	HRNet	✓		94.4
MP-GCN (Ours)	HRNet	✓		95.2
		✓	✓	95.5

Table 4: SOTA Comparison with GCNs on Volleyball and NBA datasets.

Model	#Param.	Volleyball			NBA		
		FLOPs	Pose	Pose+Obj	FLOPs	Pose	Pose+Obj
ST-GCN [68]	3.08M	4.9G	89.15	91.30	18.6G	52.00	66.8
MS-G3D [39](2-ensemble)	6.01M	18.9G	93.19	94.17	68.0G	66.34	76.23
CTR-GCN [9](4-ensemble)	5.71M	11.9G	93.56	94.54	39.0G	70.09	76.29
HD-GCN [33](6-ensemble)	7.81M	13.6G	93.71	94.91	45.2G	69.83	<u>77.39</u>
MP-GCN (Ours)	4.40M	4.2G	<u>95.21</u>	<u>95.54</u>	22.3G	72.94	75.96
MP-GCN (4-ensemble)	11.58M	13.20G	95.23	95.67	48.6G	<u>72.77</u>	78.68

3 Detailed Comparison between Keypoint-based Methods

In this section, we provide more detailed comparisons between our method and state-of-the-art keypoint-based methods on the Volleyball and NBA dataset. We also compare our method with GCNs in skeleton-based action recognition.

Table 3 presents the comparison of our method with state-of-the-art methods that leverage only keypoint information on the Volleyball dataset. With only human pose keypoints, our method achieves higher accuracy than others with even object keypoints. This result demonstrates the effectiveness of our proposed multi-person graph structure. When incorporating object keypoints, our method achieves the highest accuracy of 95.5% among all keypoint-based methods.

Table 4 presents the comparison of our method with GCNs in skeleton-based human action recognition. Each GCN adopts its original ensemble technique and single-person graph scale but includes extra ball and basketball net keypoints. All methods are evaluated using the same skeleton and object data as ours.

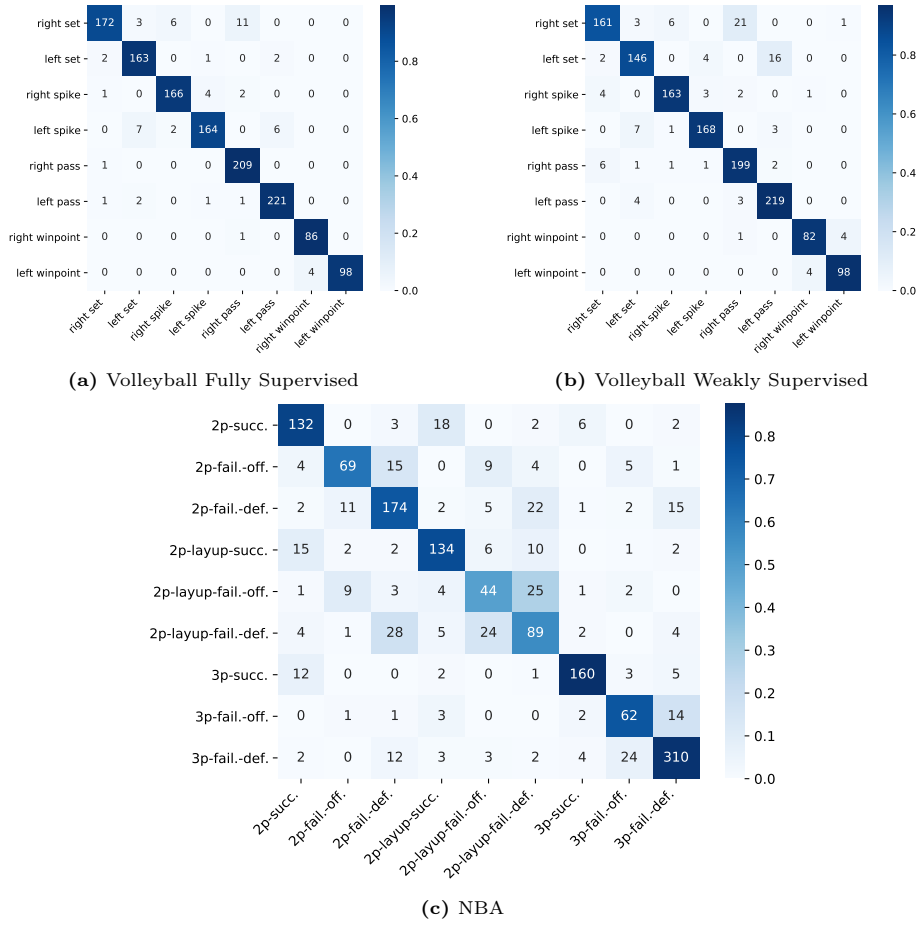


Fig. 4: The confusion matrices on Volleyball Fully Supervised, Volleyball Weakly Supervised, and NBA datasets.

Our method achieves the highest performance on both datasets when using the same ensemble technique. Simply transferring these methods to group activity recognition does not obtain the greatest performance, since they are specifically designed and tuned for single-person action recognition.

4 Additional Qualitative Results

We provide additional quantitative and qualitative results that are not included in the main paper due to page constraints.

Confusion Matrix. Figure 4 presents the confusion matrix on Volleyball Fully Supervised, Volleyball Weakly Supervised and NBA dataset. As shown in Fig. 4a, a majority samples are classified correctly, with exceptions for cases

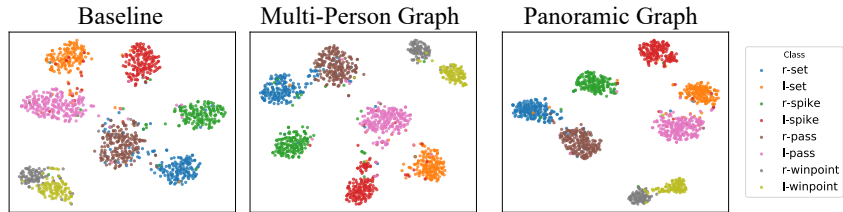


Fig. 5: t -SNE feature embedding visualization on the Volleyball dataset by different graph structure.

such as *right set* and *right pass*. For the Volleyball dataset in weakly supervised setting (Figure 4b), the overall accuracy decreases, primarily due to the confusion of *left set-left pass* and *right set-right pass*. This result may be attributed to the absence of ground-truth detection boxes, leading to missed detection and inaccurate tracking of key actors. For the NBA dataset (Figure 4c), the most confusing cases are *layup-fail.-off.-layup-fail.-def.*. These two types of actions can only be differentiated by whether the offensive or defensive team gets the rebound after the ball is thrown.

t-SNE Visualization. Figure 5 displays the t -SNE visualization of different graph structures on the Volleyball Fully Supervised dataset. It is evident that the proposed multi-person-object graph facilitates a clear separation of each class.

5 Additional Ablation Studies

In this section, we present extra ablation studies that are not included in the main paper due to page limit, including experiments on network modules, inter-body graph topologies, and input dimensions.

Table 5 illustrates the impact of different input branches and modules within the basic block. For the model that without SGC, we utilize a graph with only self-link edges as a substitute. For the model without TCN, we replace the multi-scale temporal convolution layer with a standard 5×1 temporal convolution. These results demonstrate that each component of the basic block substantially contributes to the model’s recognition capabilities.

Table 6 shows the impact of various inter-body links on the Volleyball Fully Supervised dataset. To maintain sufficient sparsity in the inter-body connections, we experiment with several connection strategies based on body centers and object keypoints. These strategies include: (1) None: No inter-body connections; (2) Fully-Connected: A fully connected graph within M body centers. (3) Linear: A linear graph with sequential connections (4) Pairwise: Connections established between pairs of individuals. The experimental results indicate that the pairwise connection strategy achieves higher accuracy. Additionally, we observed that it brings a more stable training process. In our future research, we plan to explore a broader range of topological structures for inter-body connections to potentially enhance performance further.

Table 5: Comparison of different network modules in terms of MCA on Volleyball Weakly Supervised and NBA dataset.

Module	Model Config	Volleyball	NBA
Input Branch	J	87.81	73.74
	J+B	91.47	75.24
	J+B+JM	91.92	75.53
Basic Block	w/o SGC	90.25	72.87
	w/o TCN	92.00	72.29
	w/o Attention	91.35	73.32
Ours	J+B+JM+BM	92.77	75.96

Table 6: Comparison of different inter-body links in MCA (%) on the Volleyball dataset. **Table 7:** Comparison of different input dimensions in MCA (%) on the NBA dataset.

Inter-body Graph	MCA
None	95.21
Fully-Connected	94.84
Linear	95.14
Pairwise (Ours)	95.54

Dimension	Input data	MCA
2- $\{x, y\}$	pose	68.03
	pose+object	74.48
3- $\{x, y, v\}$	pose	69.21
	pose+object	75.96

In Tab. 7, we compare the performance between 2-dimensional input ($\{x, y\}$) and 3-dimensional input ($\{x, y, v\}$) with visibility evaluation. For both types of input data, the addition of a visibility input provides more information and improves the MCA by over 1%.